Supplemental Information for "Intermittent upwelling events trigger delayed, major, and reproducible pico-nanophytoplankton responses in coastal oligotrophic waters"

R. Fuchs[1,2] *, V. Rossi[2] †, C. Caille[3] ‡, N. Bensoussan[2] §, C. Pinazo[2] ¶, O. Grosso[2] ‖, M. Thyssen[2] ††

[1]Aix Marseille Univ, CNRS, Centrale Marseille, I2M, Marseille, France

[2]Aix Marseille Univ, Université de Toulon, CNRS, IRD, MIO, Marseille, France

[3]Sorbonne Université, CNRS, LOMIC, Banyuls-sur-Mer, France

Contents of this file

1. Material and Methods details

*robin.fuchs@univ-amu.fr

†vincent.rossi@mio.osupytheas.fr

‡caillec@obs-banyuls.fr

§nathaniel.bensoussan@mio.osupytheas.fr

¶christel.pinazo@mio.osupytheas.fr

‖olivier.grosso@mio.osupytheas.fr

†† melilotus.thyssen@mio.osupytheas.fr

2. Figures S1 to S11

3. Tables S1 to S7

1. Materials and Methods Details

1.1. Stratified Period, Bloom Period and Salinity Data

1.1.1. Stratified periods characterization

The stratified period and the temperature anomalies were computed using a Butterworth digital and analog filter design (function butter of the Python "scipy.signal" subpackage). The bandwidth parameter was set to 60 days for the stratified periods determination and 15 days for the temperature anomaly. Events associated with temperature anomalies lasting less than eight hours were not considered.

1.1.2. Spring Bloom Periods Characterization

The dates of the spring bloom were determined using the threshold method (Sapiano et al., 2012; Brody et al., 2013) on the low-pass filtered biomass with a 5% threshold. The dates of the blooms in 2020 were from April 2 to April 30, 2020. There were two spring blooms in 2021, from March 25 to April 7 and from April 21 to May 12 (See Figures S4 and S5).

1.1.3. Salinity Data

The salinity data were acquired every hour using an STPS sensor from the NKE-manufacturer. Yet, salinity measurements from the STPS sensor were found not reliable and hence not used here.

1.2. Estimations of Phytoplankton Biovolume, Biomass and Growth Rates

1.2.1. Phytoplankton functional groups acquisition protocol summary

Phytoplankton organisms present significant differences in typical sizes and abundances so that two AFCM acquisition procedures are used to overcome this issue (as for example in Marrec et al. (2018)). RedPicoProk and OraPicoProk pulse shape signals were acquired by setting a low red fluorescence threshold (6 mV) and by analyzing a volume of $850\mu L$ on average whereas the RedPico, RedNano, and OraNano pulse shape signals were acquired using a high red fluorescence threshold (25 mV) and by analyzing volumes of $4000\mu L$ on average. The volume analyzed was quantified using a weight-calibrated peristaltic pump.

1.2.2. Biovolume estimation:

The biovolume of each phytoplankton cell was estimated using the relationship between AFCM Total forward scatter (the area under the FWS pulse shape) and the biovolume of Silica Beads and cell images taken by the AFCM (Figure S1). The Silica Beads were manufactured with a known size and the cell biovolumes from images were estimated according to Sun and Liu (2003). Even if the relationship existing between these two quantities is monotonic, its shape seemed not to be constant over all the possible Total FWS values. This pattern is due to the optical properties of the phytoplankton cell sizes relatively to the laser size. Indeed, for the cells exhibiting a Total FWS inferior to 2×10^2 a.u. the relationship seemed concave whereas it was convex for cells with Total FWS superior to 5×10^2 a.u. as made visible in Figure S1.

1.2.3. Biomass estimation:

The biomass ($pgC.cell^{-1}$ in the following equations) of each cell was computed from the estimated biovolume (BV, μm^3) using the following relationships:

• $Biomass = 0.260 \times BV^{0.860}$ for RedPicoProk, OraPicoProk and RedPico cells according to Menden-Deuer and Lessard (2000).

• $Biomass = 0.433 \times BV^{0.863}$ for RedNano and OraNano cells according to Verity et al. (1992).

The interquartile biovolume range of each group was:

1.3. Size-structured matrix population model

The size-structured model version introduced in Ribalet et al. (2015) was used. The corresponding code is available at `https://github.com/fribalet/ssPopModel` (version 1.1.0). By definition, the model is structured in size and the user has to define the number of classes along with a lower and upper bound of possible size for each PFG. In this study, the distribution of each PFG was discretized in 31 classes. The lower and upper bounds of a PFG size class were determined as the 1 over 1000 quantile and 999 over 1000 quantile of the PFG biovolume distribution during each SWUE, respectively. It prevented integrating outliers and avoided excluding a significant number of observations. The PFG data were linearly interpolated from a two-hour frequency to a one-hour frequency. The lightning data used by the model came from the MESURHO buoy (Cadiou et al., 2010) moored at the Rhone river mouth which is located about 40 kilometers away from the SSL@MM station. It provided the Photosynthetically Available Radiation data (PAR, $\mu E.m^{-2}.s^{-1}$) on a two hours basis. The PAR data were linearly interpolated on a 10 minutes basis. The PAR data were not available in 2021 due to a technical issue on the buoy and the growth rates were only calculated for 2019 and 2020.

1.4. PFG response identification

The rupture detection was conducted thanks to the Python "rupture" package: `https://github.com/deepcharles/ruptures`. A linear cost function with intercept was used to model the link between the water temperature and each PFG abundance or biomass signal. No observation subsampling was performed and a binary segmentation research method was used to minimize the cost function. As the goal was to identify the beginning and end of each PFG reaction, the number of rupture points was known and equal to two.

1.5. Computation of the additional biomass imputable to the Spring Bloom

The additional biomass generated between the start and the end of the bloom was computed by taking the median value over the preceding week before the bloom as a reference value. It was assumed that the biomass would have remained at this level during the whole period if the bloom did not occur. As a result, the total biomass imputable to the bloom was computed as the difference between the actual total integrated biomass and the integrated reference level. Similarly, the daily increase in biomass due to the bloom was computed by dividing the total increase by the bloom duration in days.

The additional biomass imputable to the bloom (per day or over the whole bloom) is then used as a benchmark to compare the additional biomass imputable to each SWUE. The most extreme total biomass increase started from 2021-10-20 15:00:00. The most extreme daily biomass increase during a SWUE for which we had all the phytoplankton data started on 2020-06-18 01:00:00. The actual biggest event started from 2020-09-23

19:00:00 but does not present all RedNano and OraNano points during the event and we preferred not to interpolate to have clearly estimated effects.

2. Wind-driven Upwelling/Downwelling Index

The Wind-driven Upwelling/Downwelling Index is an hourly index that uses the sea surface wind speed and direction to estimate the Ekman transport perpendicular to the coastline (Bakun, 1973). A positive index value implies that surface waters are transported offshore (due to upwelling-favorable winds); conversely, a negative index value indicates that surface waters flow onshore (denoting wind favorable to downwelling events). An upwelling event is a series of consecutive positive WUDI values. As in Odic, Bensoussan, Pinazo, Taupier-Letage, and Rossi (2022), events with average indices higher than $0.432 m^3.s^{-1}m^{-1}$ were considered as significant upwelling events. These events are associated with substantial changes in surface water temperature (more than 3°C on average, see Odic et al. (2022)), suggesting also measurable responses of both biogeochemistry (nutrients) and biology (phytoplankton). Events are considered distinct if they are separated from each other by at least one day (Millot, 1979).

References

Bakun, A. (1973). Coastal upwelling indices, west coast of north america, 1946-71. *NOAA technical report*.

Brody, S. R., Lozier, M. S., & Dunne, J. P. (2013). A comparison of methods to determine phytoplankton bloom initiation. *Journal of Geophysical Research: Oceans*, *118*(5), 2345–2357.

Cadiou, J.-F., Repecaud, M., Arnaud, M., Rabouille, C., Raimbaud, P., Radakovitch, O., ... Gaufrès, P. (2010). Mesurho: a high frequency oceanographic buoy at the rhone river mouth. In *39th ciesm congress-venice, italy, 10-14 may 2010.*

Marrec, P., Grégori, G., Doglioli, A. M., Dugenne, M., Della Penna, A., Bhairy, N., ... Thyssen, M. (2018). Coupling physics and biogeochemistry thanks to high-resolution observations of the phytoplankton community structure in the northwestern mediterranean sea. *Biogeosciences*, *15*(5), 1579–1606. Retrieved from `https://bg.copernicus.org/articles/15/1579/2018/` doi: 10.5194/bg-15-1579-2018

Menden-Deuer, S., & Lessard, E. J. (2000). Carbon to volume relationships for dinoflagellates, diatoms, and other protist plankton. *Limnology and oceanography*, *45*(3), 569–579.

Millot, C. (1979). Wind induced upwellings in the gulf of lions. *Oceanologica Acta*, *2*(3), 261–274.

Odic, R., Bensoussan, N., Pinazo, C., Taupier-Letage, I., & Rossi, V. (2022). Sporadic wind-driven upwelling/downwelling and associated cooling/warming along northwestern mediterranean coastlines. *Continental Shelf Research*, *250*, 104843.

Ribalet, F., Swalwell, J., Clayton, S., Jiménez, V., Sudek, S., Lin, Y., ... Armbrust, E. V. (2015). Light-driven synchrony of prochlorococcus growth and mortality in the subtropical pacific gyre. *Proceedings of the National Academy of Sciences*, *112*(26), 8008–8012.

Sapiano, M., Brown, C., Schollaert Uz, S., & Vargas, M. (2012). Establishing a global climatology of marine phytoplankton phenological characteristics. *Journal of Geophysical Research: Oceans*, *117*(C8).

Sun, J., & Liu, D. (2003). Geometric models for calculating cell biovolume and surface area for phytoplankton. *Journal of plankton research*, *25*(11), 1331–1346.

Verity, P. G., Robertson, C. Y., Tronzo, C. R., Andrews, M. G., Nelson, J. R., & Sieracki, M. E. (1992). Relationships between cell volume and the carbon and nitrogen content of marine photosynthetic nanoplankton. *Limnology and Oceanography*, *37*(7), 1434–1446.

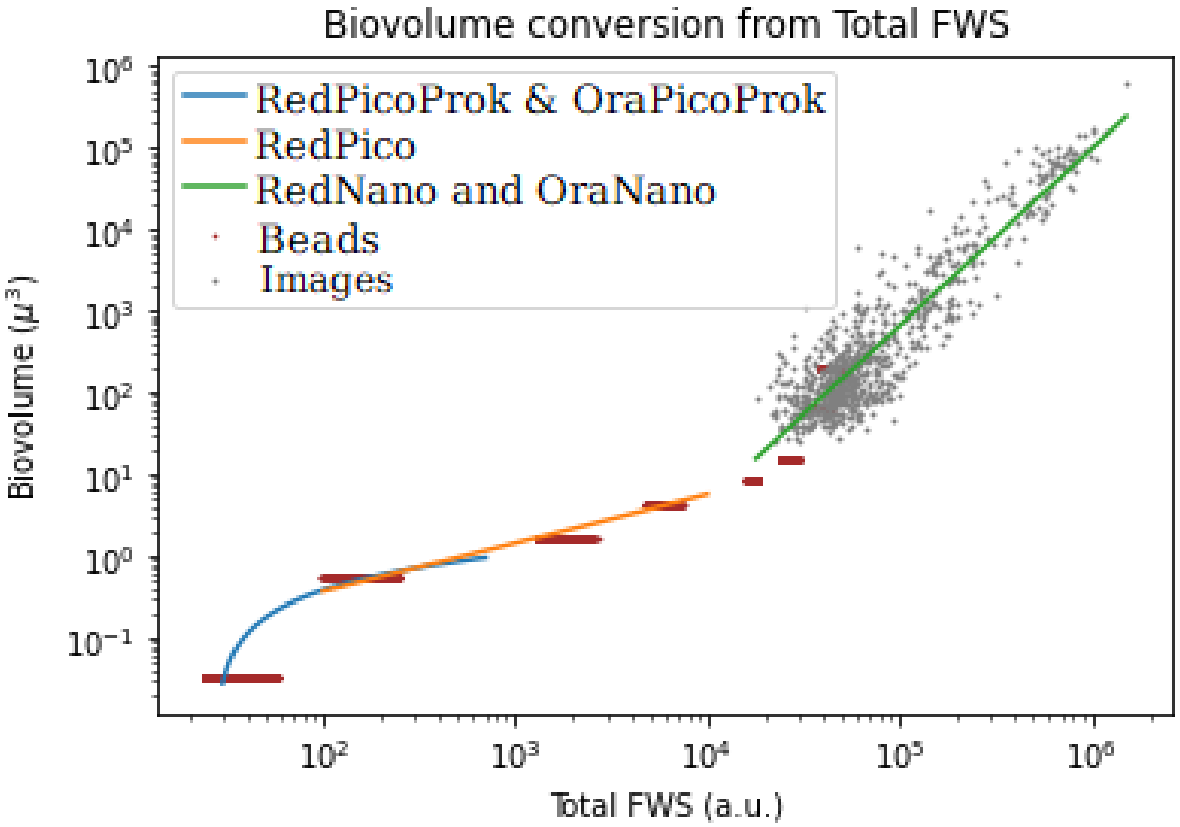

Figure S1. Summary of the empirical relationships used to convert the Total FWS signal of each cell into biovolume

	Quartile 1	Median	Quartile 3
OraNano	80.17	198.41	382.12
OraPicoProk	0.48	0.61	0.74
RedNano	10.09	25.60	60.93
RedPico	1.88	2.46	3.25
RedPicoProk	0.10	0.18	0.27

Table S1. Biovolume distribution (μm^3) (first quantile, median and third quantile) over all events (pre-reaction, reaction, and relaxation) for each PFG.

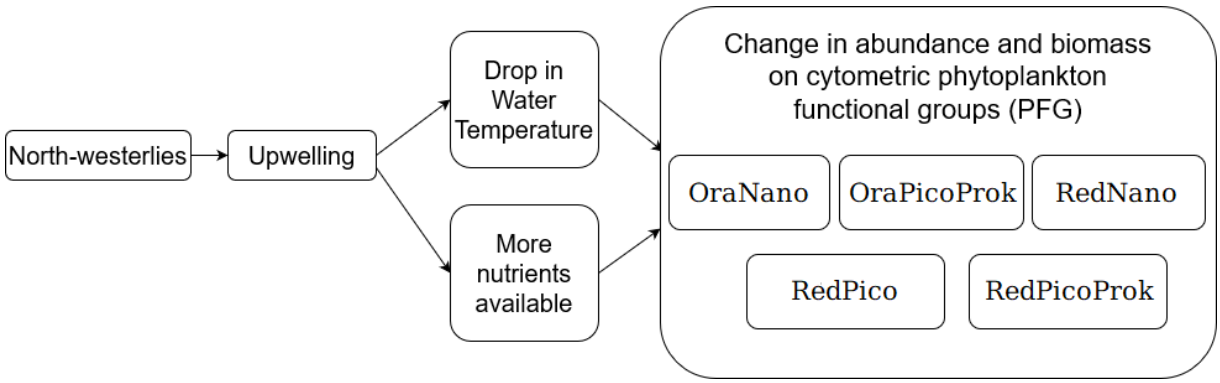

Figure S2. Summary of the causal relationships identified in this study. Reading of the underlying hydrodynamics: north-westerlies trigger offshore horizontal surface advection and upward vertical advection. Warm and nutrient-depleted surface water along with the associated phytoplankton (PFG) is exported offshore and replaced by deeper cold, nutrient-rich water, and the PFGs associated with these deeper water masses.

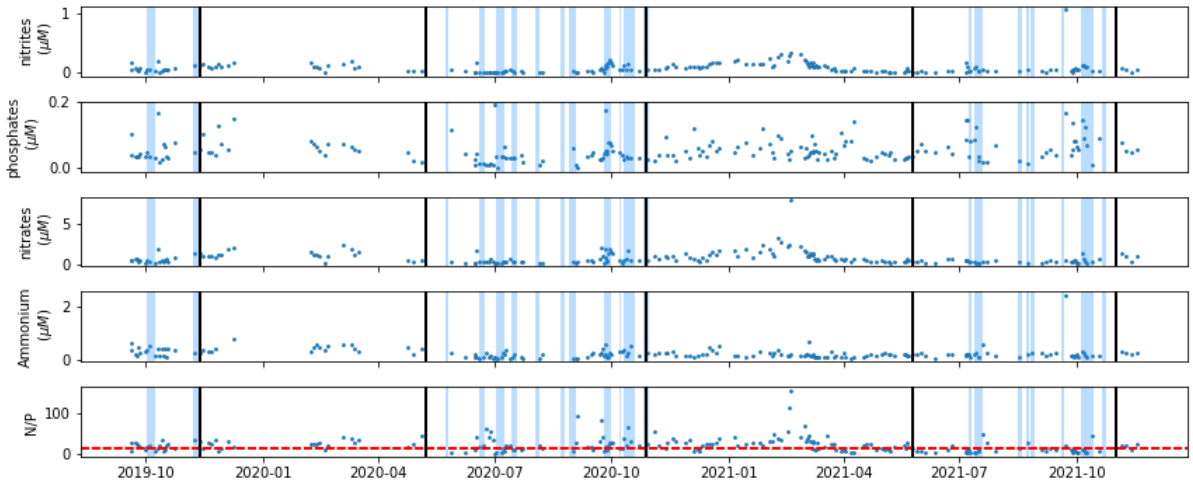

Figure S3. Nutrients over the two years of data. The colored rectangles correspond to the SWUEs considered in the study. The red dash line represents the N/P Redfield ratio (=16). The vertical black lines delimit the stratified periods (barely between early May and early November each year) from the unstratified periods.

	Unstratified	Stratified Upwelling	Stratified Non SWUE
nitrites	0.10 (0.10)	0.05 (0.09)	0.03 (0.03)
phosphates	0.05 (0.03)	0.04 (0.04)	0.04 (0.04)
nitrates	0.90 (0.77)	0.26 (0.40)	0.36 (0.27)
Ammonium	0.22 (0.16)	0.20 (0.16)	0.19 (0.12)
N/P	25.15 (16.06)	17.33 (15.72)	13.06 (14.48)

Table S2. Medians and interquartile ranges (in parentheses) of the nutrient concentrations (μM) for the nitrites, phosphates, nitrates, ammonium, and N/P ratio during the unstratified periods, the SWUEs and unstratified period excluding SWUE.

Event start	Event end	nitrates pre-anomaly	nitrates anomaly	nitrates post-anomaly	nitrites pre-anomaly	nitrites anomaly	nitrites post-anomaly	phosphates pre-anomaly	phosphates anomaly	phosphates post-anomaly	Ammonium pre-anomaly	Ammonium anomaly	Ammonium post-anomaly	N/P pre-anomaly	N/P anomaly	N/P post-anomaly
2019-09-30 21:00:00	2019-10-10 17:00:00	0.14	0.23	0.85	0.01	0.05	0.08	0.04	0.04	0.07	0.32	0.36	0.34	13.06	16.45	24.03
2019-11-06 17:00:00	2019-11-21 12:00:00		1.16	0.88		0.12	0.08		0.07	0.05		0.31	0.33		26.68	26.0
2020-05-22 14:00:00	2020-05-26 09:00:00			0.34			0.05			0.12			0.26			5.58
2020-06-18 01:00:00	2020-06-25 21:00:00	0.57	0.21	0.37	0.06	0.01	0.01	0.03	0.01	0.01	0.15	0.14	0.11	22.87	33.57	44.49
2020-06-30 23:00:00	2020-07-10 16:00:00	0.32	0.18	0.58	0.01	0.01	0.05	0.07	0.03	0.03	0.11	0.18	0.07	31.43		22.55
2020-07-14 12:00:00	2020-07-20 12:00:00	0.38	0.19	0.3	0.04	0.02	0.02	0.03	0.03	0.03	0.1	0.16	0.09	17.16	12.1	14.3
2020-07-31 18:00:00	2020-08-09 15:00:00		0.13			0.01			0.02			0.14			17.87	
2020-08-21 16:00:00	2020-08-27 20:00:00			0.35			0.03			0.06			0.06			7.3
2020-08-27 22:00:00	2020-09-05 17:00:00		0.24			0.01			0.02			0.07			43.07	
2020-09-23 19:00:00	2020-10-07 11:00:00	0.9	1.11	0.33	0.05	0.15	0.08	0.03	0.08	0.04	0.25	0.24	0.35	40.83	19.91	22.94
2020-10-06 13:00:00	2020-10-10 10:00:00	0.35		0.69	0.05		0.1	0.05		0.03	0.34		0.29	15.72		35.19
2020-10-09 16:00:00	2020-10-19 19:00:00	0.33	0.83	0.5	0.08	0.09	0.04	0.04	0.03	0.03	0.35	0.33	0.17	22.94	40.07	22.42
2020-10-25 13:00:00	2020-11-01 09:00:00	0.5	0.36	0.9	0.04	0.05	0.06	0.03	0.03	0.02	0.17	0.27	0.24	22.42	26.02	57.23
2021-07-07 02:00:00	2021-07-12 16:00:00	0.39	0.18	0.15	0.09	0.03	0.05	0.13	0.06	0.07	0.21	0.16	0.18	5.98	8.01	6.98
2021-07-11 19:00:00	2021-07-21 14:00:00	0.2	0.17	0.2	0.05	0.05	0.03	0.07	0.05	0.02	0.18	0.26	0.29	7.31	17.72	28.64
2021-08-15 02:00:00	2021-08-21 23:00:00		0.2	0.11		0.02	0.05		0.02	0.01		0.14	0.2		15.22	28.17
2021-08-21 16:00:00	2021-08-26 10:00:00		0.11			0.05			0.01			0.2	0.26		28.17	
2021-08-25 11:00:00	2021-09-02 16:00:00	0.11		0.14	0.05		0.03	0.01		0.04	0.2	0.26	0.2	28.17		9.32
2021-09-17 18:00:00	2021-09-26 13:00:00	0.22	0.41	0.33	0.05	1.06	0.04	0.04	0.17	0.08	0.25	2.47	0.15	12.66	23.34	7.54
2021-10-03 14:00:00	2021-10-16 10:00:00	0.06	0.55	0.54	0.05	0.09	0.03	0.06	0.09	0.09	0.16	0.21	0.15	4.54	16.02	7.94
2021-10-20 15:00:00	2021-10-26 11:00:00	0.54			0.03			0.09			0.15			7.94		

Table S3. Nutrients (nitrates, nitrites, ammonium, phosphates) during the three physical phases of a SWUE (pre-anomaly, anomaly, post-anomaly) for each event. Missing values correspond to events/phases that do not comply with the identifiability hypotheses stated in the Material and Methods sections of the manuscript and Supplemental Information.

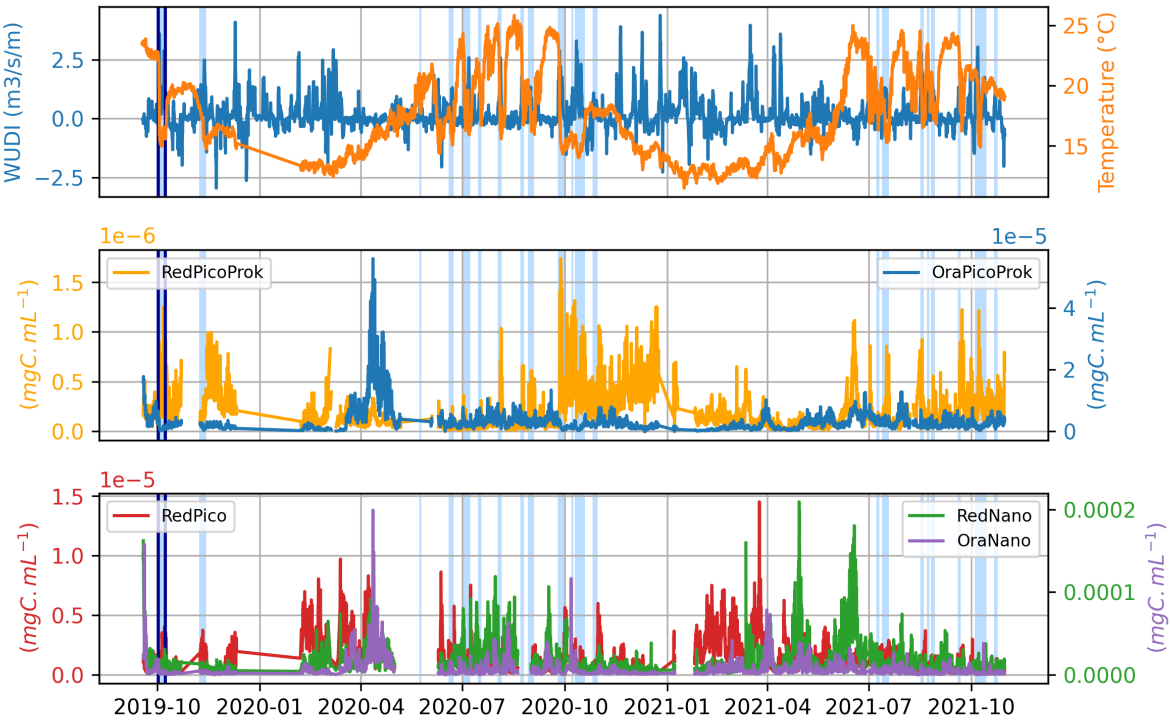

Figure S4. WUDI ($m^3.s^{-1}m^{-1}$) and temperature (C°) series (a), and phytoplankton biomass ($mgC.mL^{-1}$), at the SSL@MM station. The blue rectangles correspond to the studied SWUEs in the main text. The SWUE shown in Figure 2 in the main text is bounded by a dark blue box.

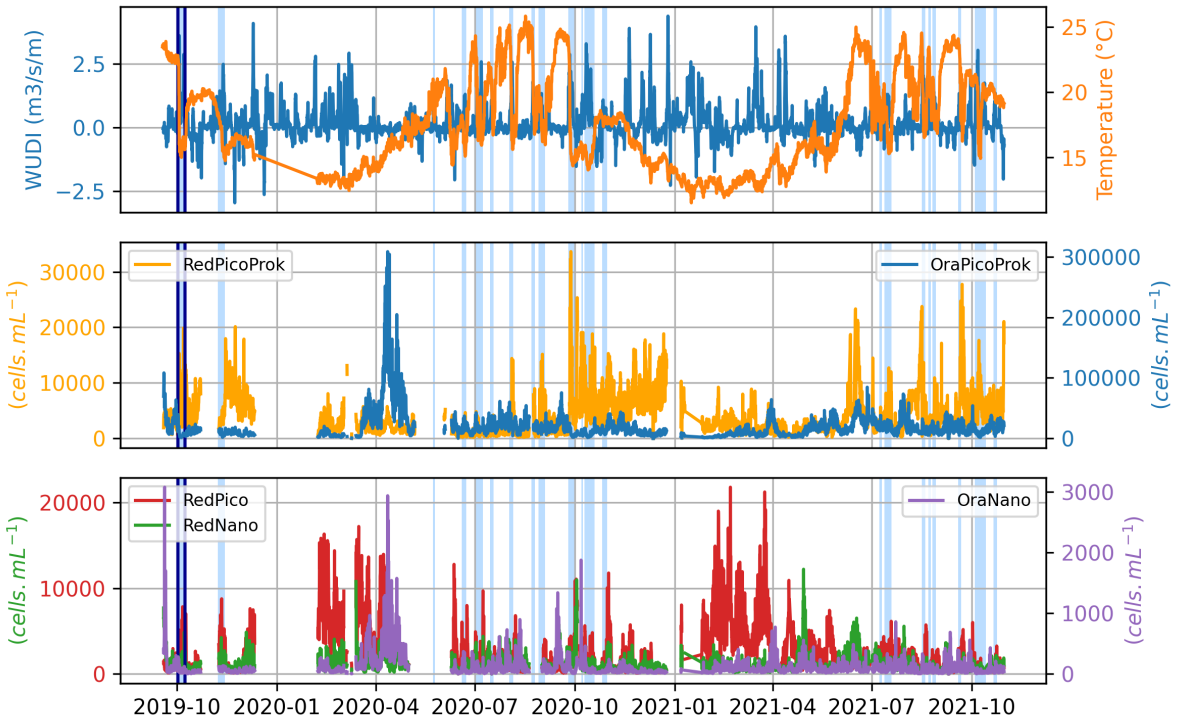

Figure S5. WUDI ($m^3.s^{-1}m^{-1}$) and temperature (C°) series (a), and phytoplankton abundances (cells.mL^{-1}), at the SSL@MM station. The blue rectangles correspond to the studied SWUEs in the main text. The SWUE shown in Figure 2 in the main text is bounded by a dark blue box.

	Unstratified	Stratified (SWUE reaction phase)	Stratified (Non SWUE)
OraNano	4.03e-06 (6.74e-06)	2.55e-06 (2.87e-06)	3.66e-06 (5.23e-06)
OraPicoProk	1.55e-06 (2.38e-06)	2.16e-06 (1.55e-06)	3.12e-06 (2.49e-06)
RedNano	8.85e-06 (9.34e-06)	9.78e-06 (8.16e-06)	1.49e-05 (1.83e-05)
RedPico	1.64e-06 (2.11e-06)	9.37e-07 (1.03e-06)	6.52e-07 (6.88e-07)
RedPicoProk	1.40e-07 (1.93e-07)	1.97e-07 (2.68e-07)	1.28e-07 (1.33e-07)

Table S4. Medians and interquartile ranges (in parentheses) of each PFG biomass (mgC.mL^{-1}) during the unstratified periods, the reaction of the PFG during SWUE, and in stratified periods outside of SWUEs.

Event start	Event end	OraNano pre-reaction	OraNano reaction	OraNano relax-ation	OraPicoProk pre-reaction	OraPicoProk reaction	OraPicoProk relax-ation	RedNano pre-reaction	RedNano reaction	RedNano relax-ation	RedPico pre-reaction	RedPico reaction	RedPico relaxation	RedPicoProk pre-reaction	RedPicoProk reaction	RedPicoProk relax-ation
2019-09-30 21:00:00	2019-10-10 17:00:00				3.19e-06	5.7e-07	1.25e-06	8.98e-06	1.282e-05	7.85e-06	8.2e-07	2.29e-06	3.7e-07	1e-07	4.6e-07	1.2e-07
2019-11-06 17:00:00	2019-11-21 12:00:00	3.08e-06	4.04e-06	1.62e-06	2.16e-06	1.07e-06	2.04e-06	1.3e-05	7.83e-06	5.45e-06	2.2e-06	1.5e-06	2.1e-07	1.8e-07	6.6e-07	4.3e-07
2020-06-18 01:00:00	2020-06-25 21:00:00	2.2e-06	7.27e-06	1.46e-06	2.06e-06	4.23e-06	2.58e-06	1.251e-05	3.578e-05	2.109e-05	1.58e-06	2.41e-06	9.9e-07	4e-08	1.9e-07	6e-08
2020-06-30 23:00:00	2020-07-10 16:00:00	5.47e-06	2.77e-06	1.23e-06	4.79e-06	3.37e-06	2.19e-06				1.19e-06	2.47e-06	6.4e-07			
2020-07-14 12:00:00	2020-07-20 12:00:00	3.36e-06	7.04e-06	1.17e-06	3.6e-06	4.21e-06	2.94e-06				7.1e-07	1.36e-06	5.5e-07	5e-08	1.1e-07	7e-08
2020-07-31 18:00:00	2020-08-09 15:00:00				6.48e-06	3.65e-06	1.86e-06	4.304e-05	1.691e-05	2.908e-05	5.8e-07	2.36e-06	6.7e-07	1e-07	2.9e-07	5e-08
2020-08-21 16:00:00	2020-08-27 20:00:00													9e-08	4.4e-07	8e-08
2020-08-27 22:00:00	2020-09-05 17:00:00	2.46e-06	5.08e-06	1.14e-06				8.75e-06	1.402e-05	1.063e-05	5.3e-07	1.75e-06	5.8e-07	7e-08	2e-07	9e-08
2020-09-23 19:00:00	2020-10-07 11:00:00	4.27e-06	7.431e-05	2.292e-05				1.065e-05	3.373e-05	1.591e-05	8.1e-07	3.53e-06	1.17e-06	7e-08	1.16e-06	3.7e-07
2020-10-06 13:00:00	2020-10-10 10:00:00										1.5e-06	8.2e-07	2.09e-06			
2020-10-09 16:00:00	2020-10-19 19:00:00				2.49e-06	1.06e-06	4.34e-06	1.554e-05	6.57e-06	1.223e-05	2.12e-06	7.2e-07	9e-07			
2020-10-25 13:00:00	2020-11-01 09:00:00	1.68e-06	5.08e-06	3.09e-06	2.15e-06	3.38e-06	5.56e-06	8.11e-06	1.578e-05	6.91e-06	6.5e-07	3.17e-06	1.86e-06	4e-07	2.5e-07	4e-07
2021-07-07 02:00:00	2021-07-12 16:00:00	4.57e-06	3.16e-06	2.18e-06	3.32e-06	4.56e-06	3.01e-06	1.992e-05	1.441e-05	1.987e-05	1.12e-06	1.37e-06	2.18e-06	9e-08	1.2e-07	1e-07
2021-07-11 19:00:00	2021-07-21 14:00:00	1.98e-06	4.34e-06	1.88e-06	2.41e-06	3.02e-06	1.55e-06				1.28e-06	2.11e-06	9.2e-07	1.5e-07	2.7e-07	6e-08
2021-08-15 02:00:00	2021-08-21 23:00:00				1.4e-06	5.13e-06	1.91e-06	1.377e-05	6.38e-06	9.51e-06	3.9e-07	1.94e-06	4.3e-07	6.9e-07	1.9e-07	1.5e-07
2021-08-21 16:00:00	2021-08-26 10:00:00	1.35e-06	5.81e-06	2.76e-06	1.43e-06	2.59e-06	3.19e-06	6.04e-06	8.93e-06	1.482e-05	2.8e-07	7.5e-07	1.25e-06	1.1e-07	9e-08	1.5e-07
2021-08-25 11:00:00	2021-09-02 16:00:00	4.26e-06	2.07e-06	7.9e-07	3.12e-06	2.4e-06	1.47e-06				8.3e-07	1.16e-06	4.4e-07	1.2e-07	2e-07	1.1e-07
2021-09-17 18:00:00	2021-09-26 13:00:00				3.41e-06	2.17e-06	9.3e-07	6.38e-06	9.78e-06	3.39e-06	6.9e-07	1.81e-06	2.1e-07	1.6e-07	5e-07	1.3e-07
2021-10-03 14:00:00	2021-10-16 10:00:00	1.06e-06	2.839e-05	1.14e-06	2.47e-06	1.38e-06	2.39e-06	5.22e-06	1.084e-05	8.15e-06				2.1e-07	5.4e-07	1.9e-07
2021-10-20 15:00:00	2021-10-26 11:00:00	1.41e-06	3.75e-06	1.42e-06				5.5e-06	1.032e-05	6.86e-06	2.2e-07	9.2e-07	4.3e-07	1.9e-07	5.1e-07	2e-07

Table S5. PFG biomass (mgC.mL^{-1}) during the three response phases of a SWUE (pre-reaction, reaction, relaxation) for each event. Missing values correspond to events/phases that do not comply with the identifiability hypotheses stated in the Material and Methods sections of the manuscript and Supplemental Information.

	Unstratified	Stratified (SWUE reaction phase)	Stratified (Non-SWUE)
OraNano	69.21 (97.68)	58.19 (62.24)	77.73 (90.02)
OraPicoProk	8706.83 (14998.82)	13161.05 (9739.31)	18633.22 (15789.77)
RedNano	881.50 (853.54)	908.64 (634.03)	1052.81 (1013.43)
RedPico	2775.45 (4229.14)	1612.28 (1866.72)	997.38 (1019.65)
RedPicoProk	2734.51 (3167.50)	4267.94 (5349.91)	2988.55 (3747.08)

Table S6. Medians and interquartile ranges (in parentheses) of each PFG abundance (cells.mL^{-1}) during the unstratified periods, the reaction of the PFG during the SWUEs, and in stratified periods outside of SWUEs.

Event start	Event end	OraNano pre-reaction	OraNano reaction	OraNano relax-ation	OraPicoProk pre-reaction	OraPicoProk reaction	OraPicoProk relax-ation	RedNano pre-reaction	RedNano reaction	RedNano relax-ation	RedPico pre-reaction	RedPico reaction	RedPico relax-ation	RedPicoProk pre-reaction	RedPicoProk reaction	RedPicoProk relaxation
2019-09-30 21:00:00	2019-10-10 17:00:00	120.36	48.91	11.34	18822.68	4720.44	8958.55	748.34	1476.27	534.29	976.98	3639.93	576.44	2049.18	8566.11	1066.59
2019-11-06 17:00:00	2019-11-21 12:00:00	86.71	70.98	39.97	11915.63	5569.7	10953.95	1229.45	1005.83	658.78	4588.86	2995.21	401.26	2997.64	4238.25	10115.57
2020-06-18 01:00:00	2020-06-25 21:00:00	51.7	49.4	12.45	12419.94	20174.36	13201.1	650.01	814.08	978.17	2559.85	4276.97	1286.45	639.97	1078.09	939.68
2020-06-30 23:00:00	2020-07-10 16:00:00	91.72	51.24	17.44	25972.71	15628.82	11251.28	1751.22	925.64	914.29	2414.35	1639.85	813.2	1142.63	1061.83	935.6
2020-07-14 12:00:00	2020-07-20 12:00:00	59.2	84.88	16.44	20150.33	21343.31	14918.93	1465.89	1045.98	1013.86	965.03	1198.32	652.03	819.59	1649.34	914.32
2020-07-31 18:00:00	2020-08-09 15:00:00	124.86	79.16	74.75	28611.35	20943.59	10443.27	1690.09	1180.91	901.56	800.93	2404.58	780.99	1471.8	5664.63	1005.76
2020-08-21 16:00:00	2020-08-27 20:00:00				23407.85	38826.92	18628.38							1020.29	4025.25	1029.43
2020-08-27 22:00:00	2020-09-05 17:00:00	86.27	21.75	21.85	14482.75	20407.14	13582.27	841.11	1234.32	684.88	798.91	2883.31	701.83	1087.02	4090.3	1504.48
2020-09-23 19:00:00	2020-10-07 11:00:00	218.32	78.25	100.23	18253.94	4927.48	8806.19	1455.73	2307.71	1062.98	1289.34	1783.04	4728.91	1368.21	21480.04	7802.58
2020-10-06 13:00:00	2020-10-10 10:00:00										3029.82	2215.24	4962.67			
2020-10-09 16:00:00	2020-10-19 19:00:00	155.81	40.05	58.94	13459.41	5739.92	25850.43	604.28	626.33	1057.79	3543.82	1590.15	1525.75	11875.27	5184.72	9140.39
2020-10-25 13:00:00	2020-11-01 09:00:00	37.73	31.99	69.23	17496.22	10661.45	22075.97	719.7	3090.65	1355.27	1125.33	3702.52	6566.14	7744.15	4664.43	7807.99
2021-07-07 02:00:00	2021-07-12 16:00:00	87.67	82.71	50.7	20156.53	33707.92	18902.32	1522.9	1062.6	1157.4	1718.07	2326.16	3285.49	2387.81	3110.83	3233.78
2021-07-11 19:00:00	2021-07-21 14:00:00	45.83	122.19	45.72	15749.11	18739.53	9047.63	776.33	1029.5	724.42	2447.86	2532.27	1260.2	4276.27	5229.57	1891.26
2021-08-15 02:00:00	2021-08-21 23:00:00	38.81	53.49	16.61	8261.14	23696.82	11825.82	737.91	664.25	541.71	458.78	1461.43	572.7	20232.91	1931.79	3606.75
2021-08-21 16:00:00	2021-08-26 10:00:00	36.6	76.56	66.65	8378.33	16030.61	21994.74	355.21	621.39	782.38	370.59	1366.14	1829.49	2718.37	1946.73	2333.22
2021-08-25 11:00:00	2021-09-02 16:00:00	65.99	48.98	16.34	19933.48	14944.28	9338.56	986.4	687.62	384.95	1890.49	1487.4	517.95	2372.58	4924.45	2717.74
2021-09-17 18:00:00	2021-09-26 13:00:00	82.42	85.49	41.5	14205.01	19966.8	6019.29	581.78	985.85	253.57	1175.69	3455.8	328.26	4732.87	12118.97	3641.71
2021-10-03 14:00:00	2021-10-16 10:00:00	46.04	29.33	33.71	11502.6	7313.59	15506.97	541.14	863.64	538.03	383.29	952.05	448.88	5218.97	9735.04	4808.44
2021-10-20 15:00:00	2021-10-26 11:00:00	44.49	25.04	78.67				597.69	1565.21	1122.46	375.75	1873.8	806.56			

Table S7. PFG abundances (cells.mL^{-1}) during the three response phases of a SWUE (pre-reaction, reaction, relaxation) for each event. Missing values correspond to events/phases that do not comply with the identifiability hypotheses stated in the Material and Methods sections of the manuscript and Supplemental Information.

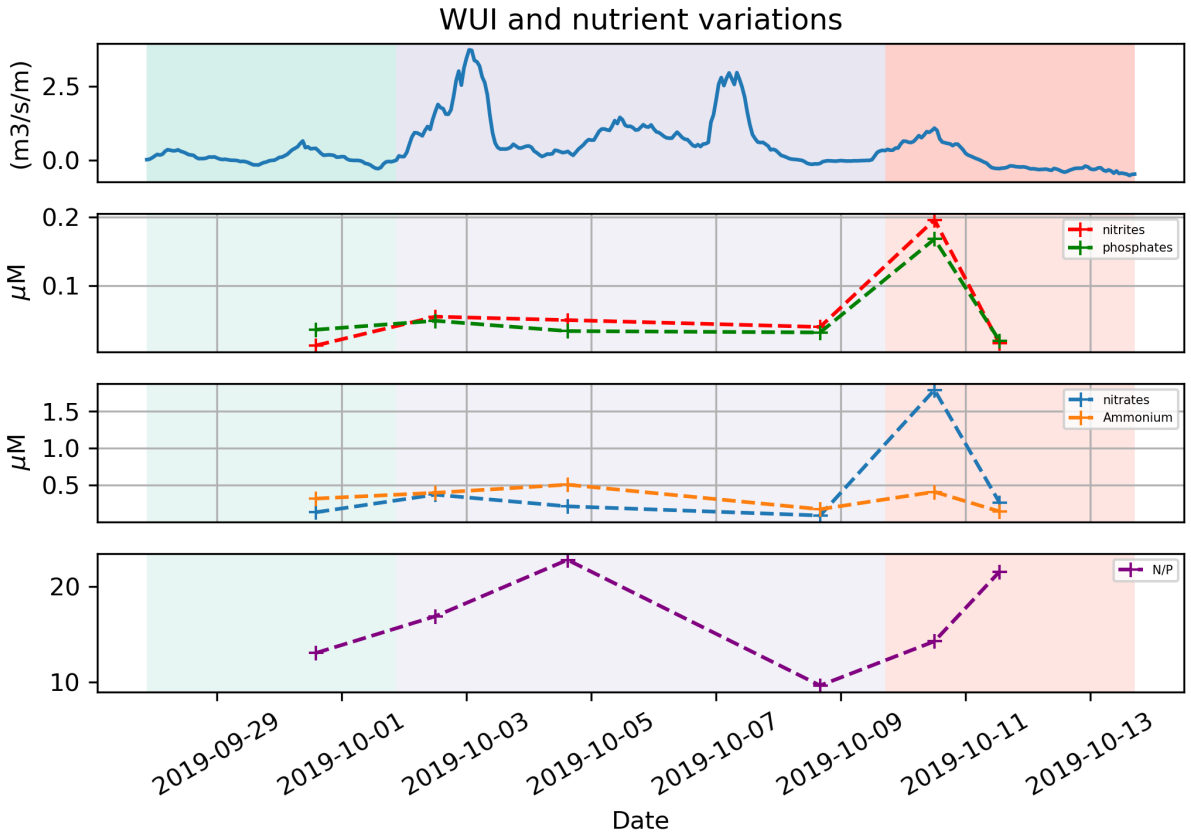

Figure S6. Nutrients and N/P ratio during the SWUE shown in Figure 2 in the main text.

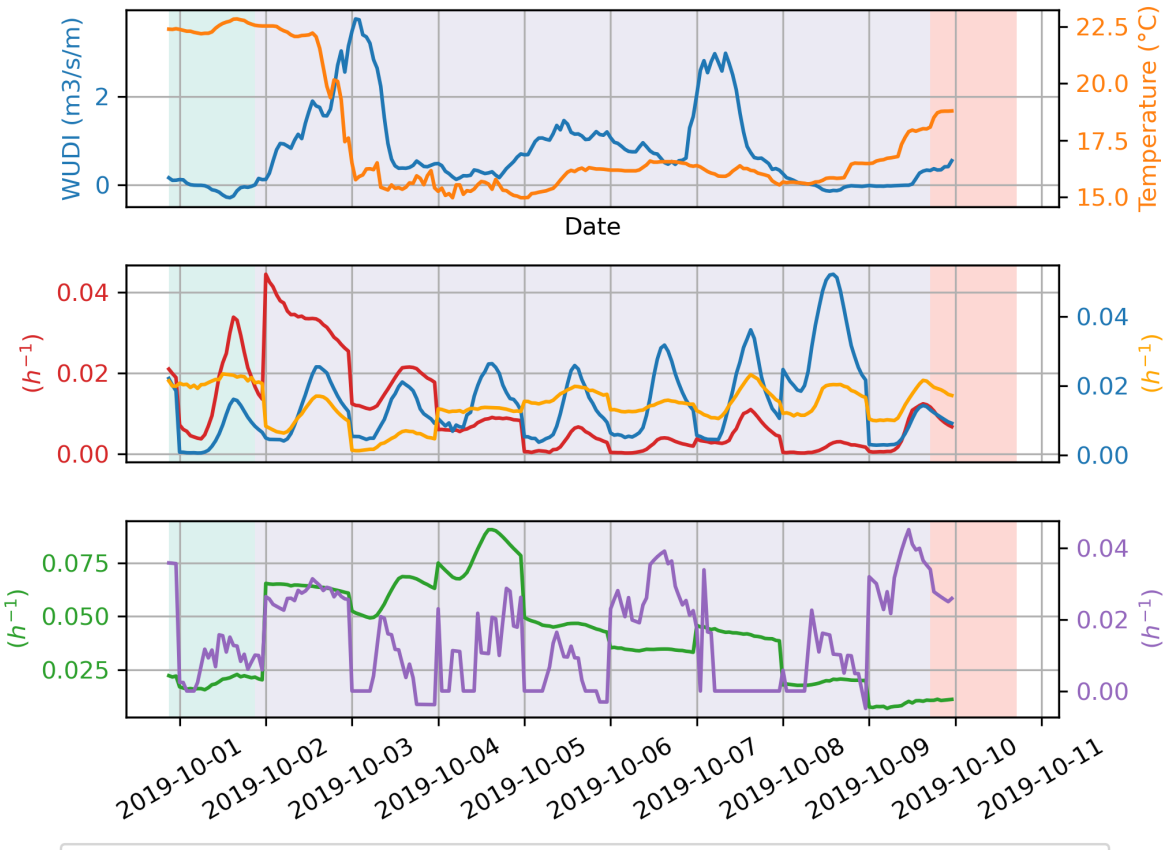

Figure S7. Hourly growth rates during the SWUE shown in Figure 2 in the main text.

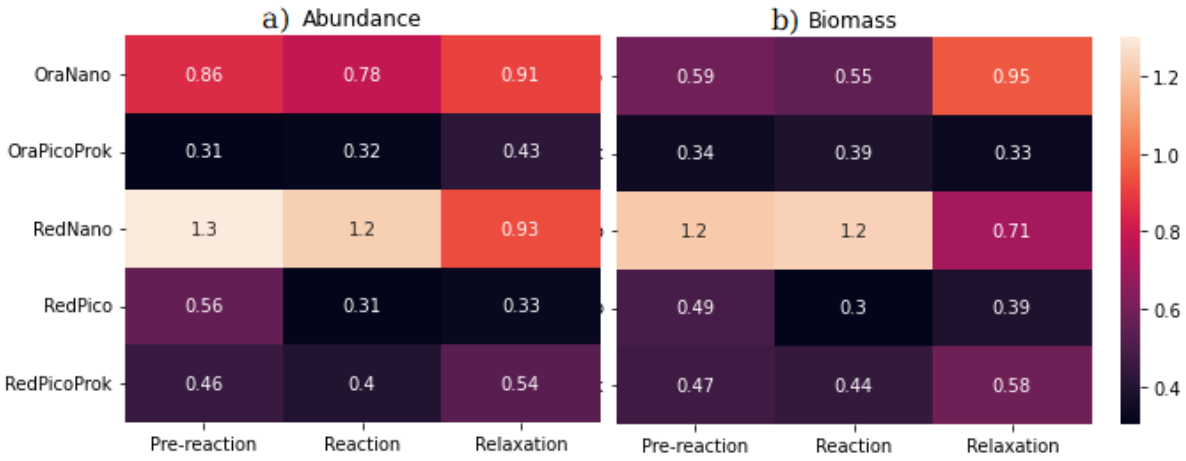

Figure S8. Estimated PFG daily growth rates during the three biological phases as defined by the abundance rupture points (a) or biomass rupture points (b). Only the RedPico growth rates significantly differed between the phases (for both abundance and biomass rupture points) and the RedNano using the biomass rupture points (Kruskal-Wallis test, p-value ≤ 0.05)

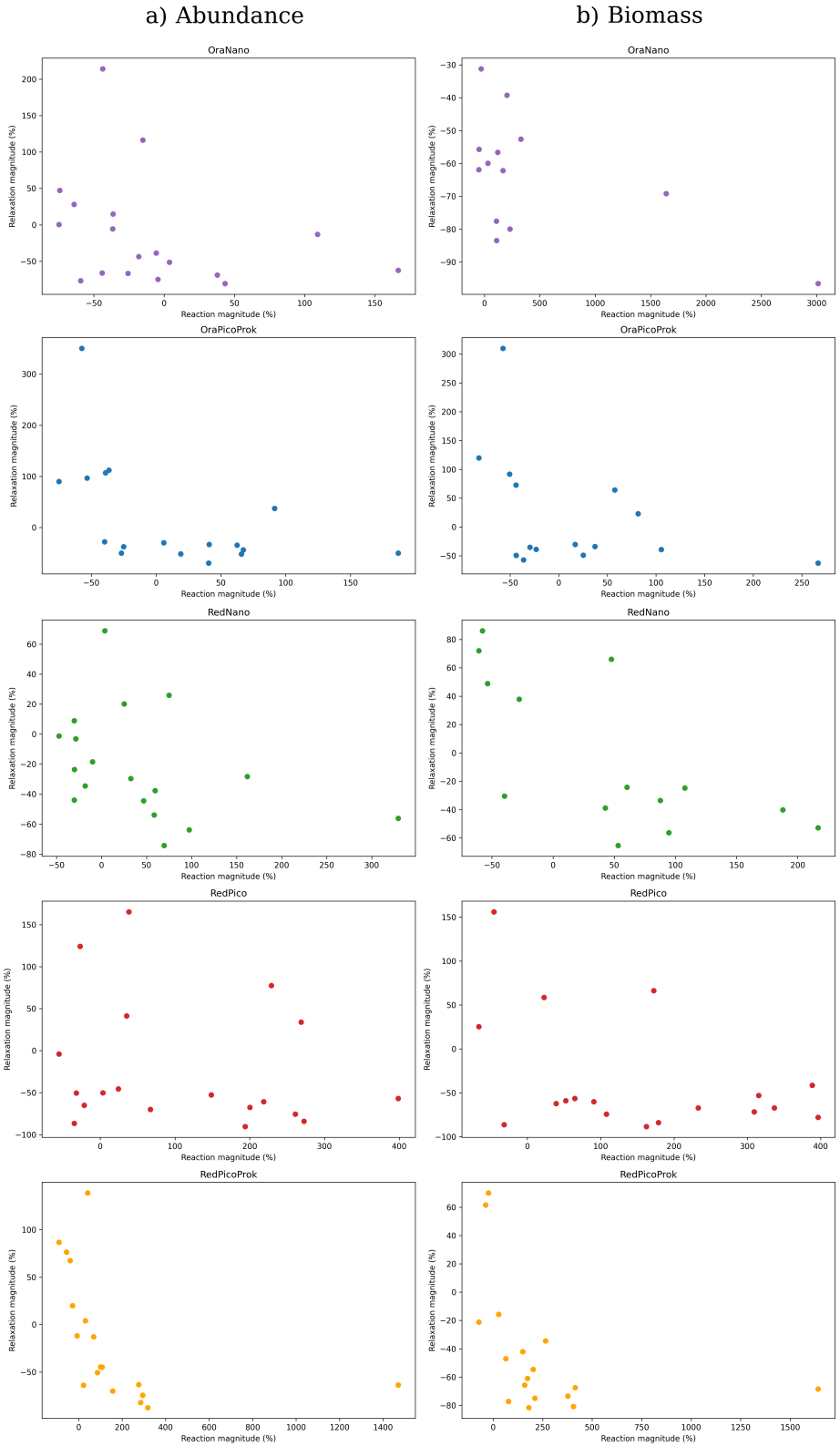

Figure S9. Inverse relationship existing between relaxation and reaction phases for all PFGs in both abundance (a) and biomass (b) illustrating a catch-up phenomenon.

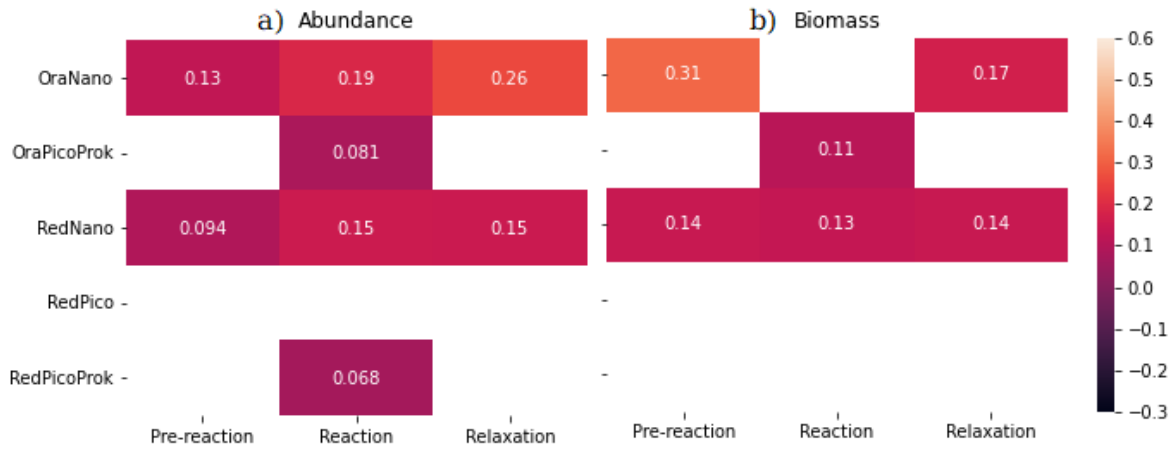

Figure S10. Spearman correlations between estimated growth and loss rates using the abundance (a) and biomass (b) rupture points for all PFG before their reaction, during their reaction and during their relaxation phase. Only correlations significant at 5% are displayed. The number of observations on which these correlations are computed is given in Figure 3 in the main text.

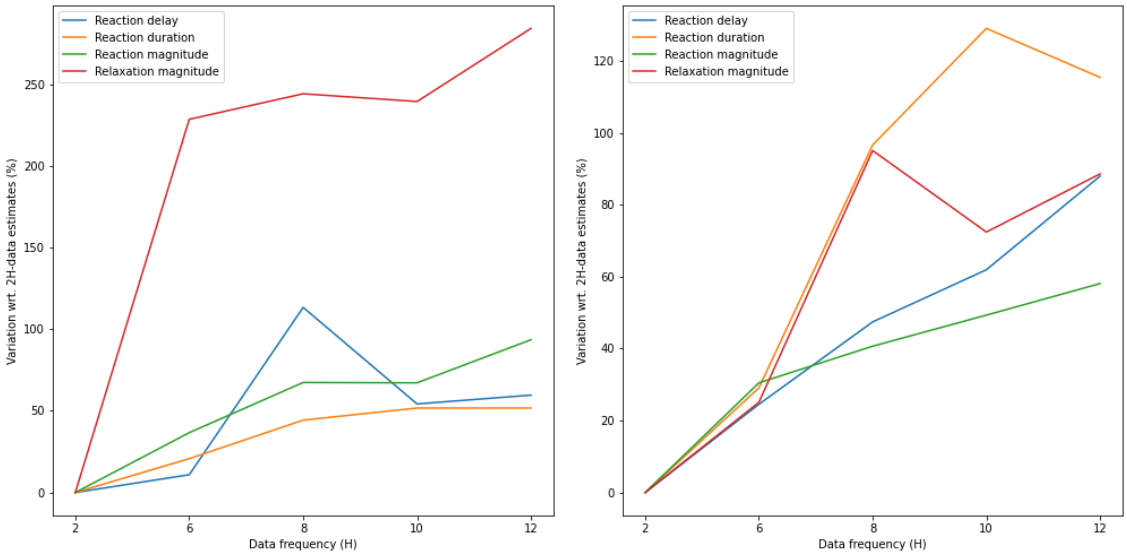

(a) Abundance (b) Biomass

Figure S11. Absolute variations of the estimations of the four main quantities of interest (reaction delay, reaction magnitude, reaction duration and relaxation magnitude) for both abundance (a) and biomass (b) due to a change in the data frequency. The original 2h-frequency data have been subsampled to obtain 4h-frequency to 12h-frequency versions of the dataset. Then the model has been run on each data frequency and the variation percentage of the estimates with respect to the 2h dataset was computed by averaging over all PFGs and events. Data frequency hence strongly influences the results especially, for frequencies lowest than 6 hours.

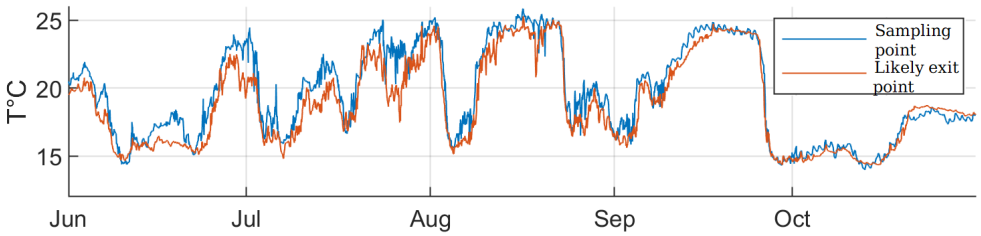

(a) SSL@MM-exit point during the whole 2020 year

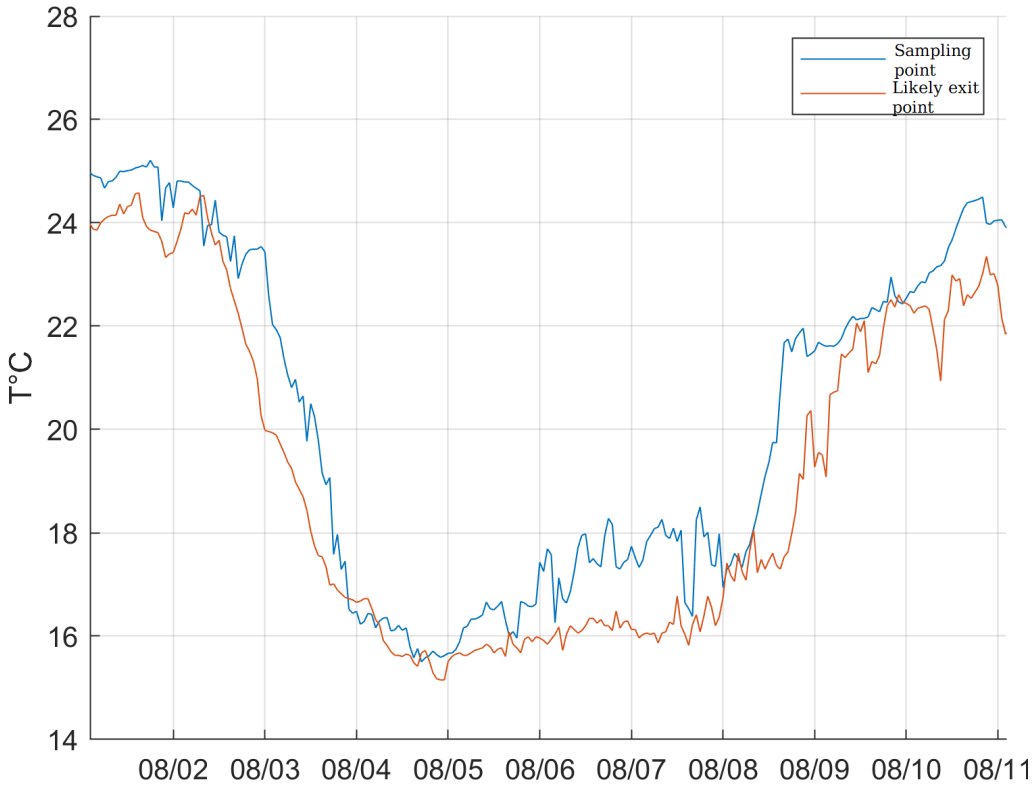

(b) SSL@MM-exit point during an event in August 2020

Figure S12. Comparison between the potential exit point and sampling points temperatures, during the whole 2020 year (a) and during an example in August 2020 event (b).
Interpretation: The likely exit point of the presented SWUEs is at ∼30 kilometers from the station (Odic et al., 2022). The correlations between the WUDI indices computed at this point and for the Marseille coastline (>95%, p-value<0.01, results not shown) show that the upwelling forces at stake could be considered homogeneous along the coastline. Similarly, the comparison on 2020 of the SSL@MM station *in situ* temperature and the temperature near the exit point shows how similar they are. This is the case in general (a) and during each SWUE for which an example is given in Figure b). In b), the sampling site and the exit site present the same water drop magnitudes with a small lag (<8 hours): The water masses advection to the sampling site is short.